ACS SENSORS

pubs.acs.org/acssensors

Article

β-Sheet Richness of the Circulating Tumor-Derived Extracellular Vesicles for Noninvasive Pancreatic Cancer Screening

Komila Rasuleva, Santhalingam Elamurugan, Aaron Bauer, Mdrakibhasan Khan, Qian Wen, Zhaofan Li, Preston Steen, Ang Guo, Wenjie Xia, Sijo Mathew, Rick Jansen, and Dali Sun*

Cite This: *ACS Sens.* 2021, 6, 4489−4498

Read Online

ACCESS | Metrics & More | Article Recommendations | Supporting Information

ABSTRACT: Tumor-derived extracellular vesicles (EVs) are under intensive study for their potential as noninvasive diagnosis biomarkers. Most EV-based cancer diagnostic assays trace supernumerary of a single cancer-associated marker or marker signatures. These types of biomarker assays are either subtype-specific or vulnerable to be masked by high background signals. In this study, we introduce using the β-sheet richness (BR) of the tumor-derived EVs as an effective way to discriminate EVs originating from malignant and nonmalignant cells, where EV contents are evaluated as a collective attribute rather than single factors. Circular dichroism, Fourier transform infrared spectroscopy, fluorescence staining assays, and a de novo workflow combining proteomics, bioinformatics, and protein folding simulations were employed to validate the collective attribute at both cellular and EV levels. Based on the BR of the tumorous EVs, we integrated immunoprecipitation and fluorescence labeling targeting the circulating tumor-derived EVs in serum and developed the process into a clinical assay, named EvIPThT. The assay can distinguish patients with and without malignant disease in a pilot cohort, with weak correlations to prognosis biomarkers, suggesting the potential for a cancer screening panel with existing prognostic biomarkers to improve overall performance.

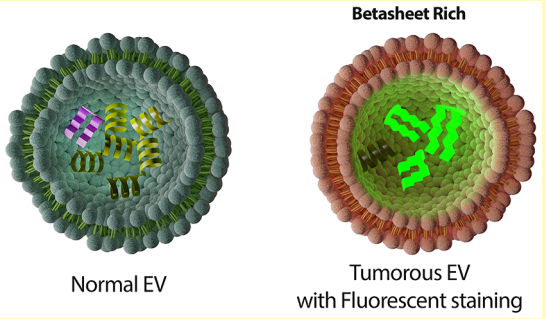

KEYWORDS: *extracellular vesicles, protein structure, β-sheet, collective attribute, PDAC*

Extracellular vesicles (EVs), which contain biomolecules from parental cells, play important roles in cell−cell signaling,[1−4] immune response,[5] and metastasis.[6,7] EVs have been recognized as an excellent biomarker reservoir for the detection of many types of cancers, including colorectal, breast, and pancreatic cancer.[8−14] EVs released into circulation are under intensive investigation to tap the theoretical potential as noninvasive detection biomarkers for their preponderance compared with other candidates such as circulating tumor cells.[15−17] Most of these studies focus on EV single protein/RNA/mutant DNA allele or molecular signatures based on multiplex assays, but such markers are problematic since they are either subtype-specific leading to false-negative or easily masked by high background signals in the liquid biopsy, leading to false-positives.[18,19] To date, none of the candidate markers have been approved for cancer screening in clinical practice, which underlies the problem in many liquid biopsy studies including the current EV marker discovery approaches. Translating disease-derived EVs into biomarkers has also been challenging due to the lack of simple methods for EV analysis. Conventional detection technologies require time-consuming and labor-intensive isolation and purification procedures (e.g., ultracentrifugation or multistep filtration), followed by EV quantification and/or analyses of EV molecular contents.[4,20−22] The common practice of EV quantitation is through scattering-based nanoparticle tracking analysis (Nanosight) or tunable resistive pulse sensing (qNano), which are counting-based quantification bearing considerable variations.[23−28] Most of these techniques would be impractical for clinical use since they require relatively large sample volumes, are complex, low-throughput, and expensive, and have long turnaround times.

Protein quantification and analysis are well-accepted approaches for EV-based biomarker discovery but limited to the identification without structural information. We studied the collective attribute of EV by analyzing the secondary structure of the EV proteins using circular dichroism (CD), Fourier transform infrared (FT-IR), and fluorescent staining rather than single biomarkers. We found malignant cell secretes more β-sheet-rich proteins into EVs than their nonmalignant counterparts. Theoretical rationale integrating proteomics, bioinformatics, and protein folding simulation also concluded the β-sheet richness (BR) of the malignant cells and EVs considering the individual proteins' contributions. Furthermore,

Received: September 21, 2021
Accepted: November 15, 2021
Published: November 30, 2021

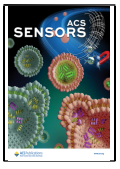

https://doi.org/10.1021/acssensors.1c02022
ACS Sens. 2021, 6, 4489−4498

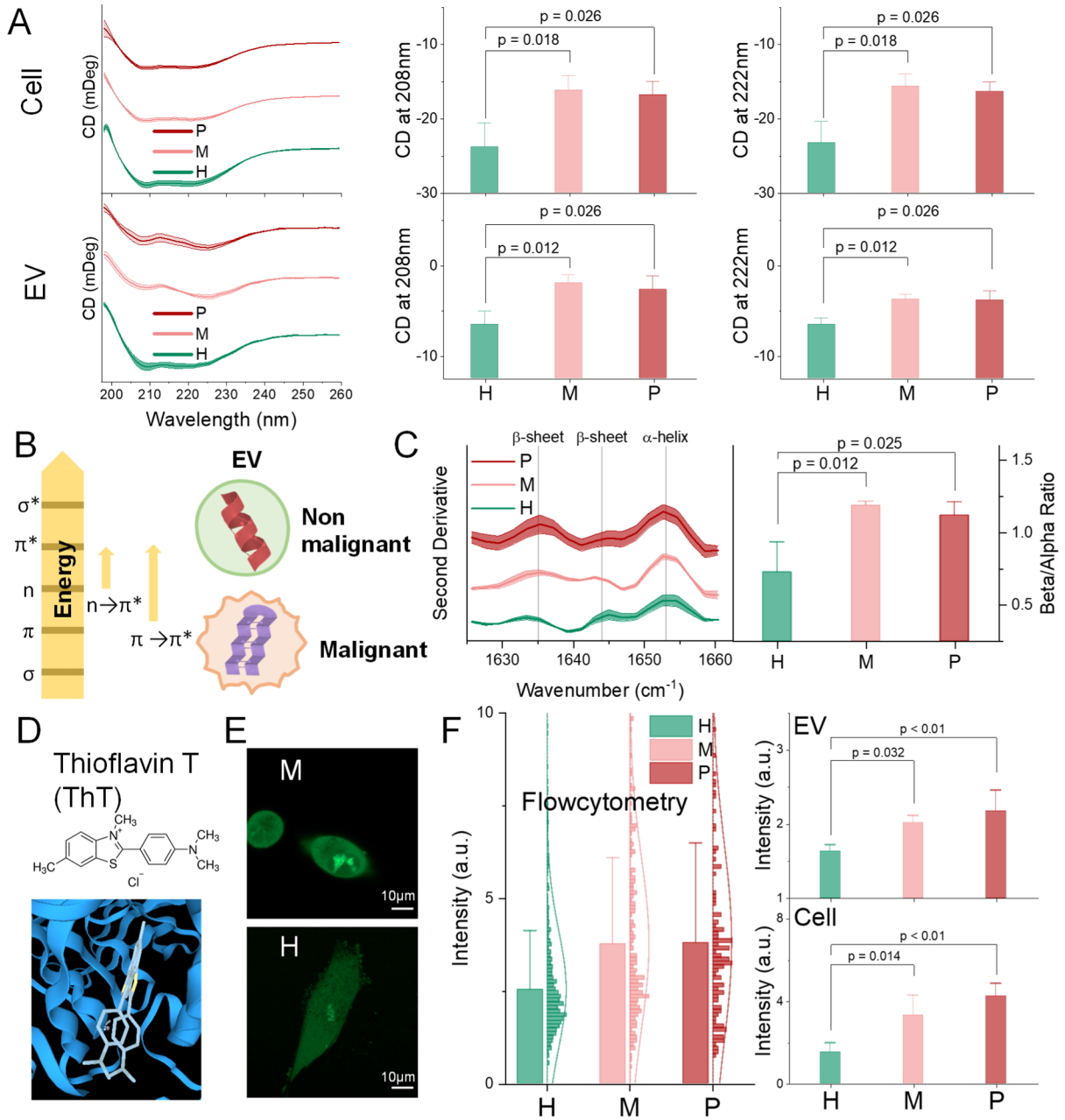

Figure 1. β-sheet richness (BR) is a feature of PDAC cells and EVs. (A) CD spectra (stacked), peak value at 222 and 208 nm (due to $\pi \rightarrow \pi^*$ and n $\rightarrow$ π^* transition, respectively) of the cellular and EV proteins' CD spectra at a protein concentration of 0.5 and 0.2 mg/mL, respectively. (B) Absorption involves the promotion of an electron to a higher state (left), and a schematic cartoon of the α-helix-rich normal EVs and β-sheet-rich tumorous EVs (right). (C) Second derivative IR spectra (left) of amide I region for protein secondary structure accessing, and relative intensities of amide I bands providing the spectroscopic β-sheet-to-α-helix ratio (right). (D) Chemical structure of ThT and its binding example to β-sheets (adapted from 3decision.discngine.com). (E) Confocal micrographs of cells stained with 50 nM ThT. Scale bars represent 10 μm. (F) Flow cytometry measurement of ThT-stained cells (left). Fluorescence intensity of the ThT-stained proteins from cellular and EV lysates (right). H: HPNE; M: MIA PaCa-2; and P: PANC-1. Error bars, mean $\pm$ s.e.m; n = 3; n.s., not significant; and p values were determined by unpaired two-tailed t-tests.

the theoretical validation workflow highlighted an extended analysis combining protein−protein interaction and enrichment analysis, providing unprecedented opportunities to interrogate the stereochemical features associated with malignancy.

Krafft et al. introduced the secondary structural signature of EV as a cancer screening marker.[29] However, intricated equipment (FT-IR and Raman spectrometry) and EV purification requirements hinder further translational development. To develop a cancer screening assay targeting BR of circulating tumor-derived EVs, we designed a protocol integrating immunoprecipitation (IP) and fluorescence detection, named EvIPThT. The assay readout of a retrospective pilot cohort showed sufficient discriminatory power comparing samples from cancer cases, disease controls and healthy donors, and a weak correlation to the concurrent prognosis biomarkers. Since no BR change was observed in the chemo-treated malignant cells compared with nontreated ones, the simple, inexpensive, low sample (100 μL) and time consumption (1 h), high-throughput, and automatable EvIPThT assay shows

https://doi.org/10.1021/acssensors.1c02022
ACS Sens. 2021, 6, 4489−4498

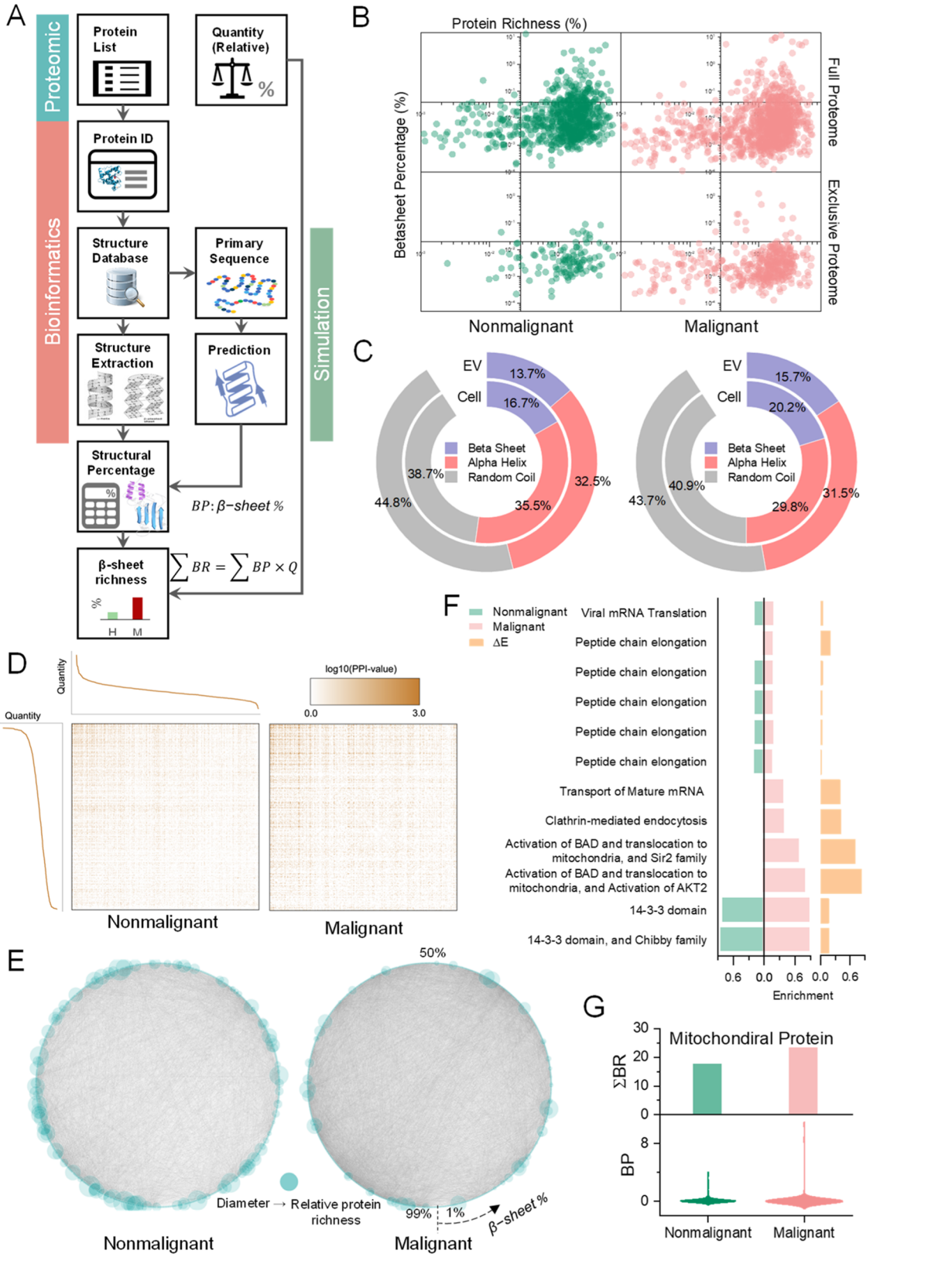

Figure 2. BR analysis by combining proteomics, bioinformatics, and simulations. (A) BR analysis workflow. (B) Scatter plot paring β-sheet percentage (BP) and protein richness (Q). (C) Protein structural constitute of cells at cellular and EV levels. (D) PPI heat map sorted by the relative quantity of the proteins (Q). Each node (x and y axes) represents a protein ranked by relative protein quantity (Q). n = 1,103,777 for malignant and nonmalignant cells, respectively. (E) Circular PPI network graphs sorted by BP. Node size represents Q. (F) Comparative GO term enrichment analysis result. ΔE denotes the enrichment score difference between malignant and nonmalignant cells. Terms in the LNC category with $\Delta E > 0$ were shown. (G) BR (top) and BP distribution (bottom) of the mitochondrial proteins. Nonmalignant: HPNE; Malignant: MIA PaCa-2.

https://doi.org/10.1021/acssensors.1c02022
ACS Sens. 2021, 6, 4489−4498

promise as a cancer screening assay, filling the translational gaps left by current EV detection applications.

RESULTS

Tumorous EV Proteins Are β-Sheet-Rich. CD spectroscopy, defined as the unequal absorption of left-handed and right-handed circularly polarized light, is a sophisticated and excellent indicator for rapidly evaluating the secondary structure and folding and binding properties of proteins.[30] Secondary structural elements of protein (α-helix and β-sheet and random coil) have their CD spectra features. However, CD analysis targets mostly purified single proteins and peptides.[31] Using CD for characterizing EV proteins is underexplored. Thus, we designed and optimized an experimental protocol for characterizing EV using CD measurement. We analyzed EVs isolated from three pancreas cell lines: a cell line derived by immortalization of primary ductal pancreas cells [HPNE (H), nonmalignant] and two representative primary pancreatic ductal adenocarcinoma (PDAC) cell lines (malignant) with different genotypes [PANC-1 (P) and MIA PaCa-2 (M)]. We observed significant differences in the CD spectrum between malignant and non-malignant at both cellular and EV levels (Figure 1A). By scrutinizing the far-UV spectra, non-malignant cells and EVs presented profiles similar to a typical α-helix abundant protein, while malignant counterparts presented a classic β-sheet-abundant protein profile.[32] Therefore, we hypothesized that α-helix is richer in non-malignant EVs, whereas β-sheets are richer in tumorous EVs (schemed in Figure 1B). It is comparatively easy to validate the α-helix richness in non-malignant EVs because α-helix is featured by negative bands at 222 and 208 nm and due to $\pi \rightarrow \pi^*$ and $n \rightarrow \pi^*$ transition, respectively (Figure 1B).[33] The corresponding negative level of these two peaks (Figure 1A) verified the first hypothesis that nonmalignant compared to malignant cells are richer in α-helix at both the cellular and EV levels. Such an $n \rightarrow \pi^*$ transition, involving protein carbonyl and amide groups, has been estimated to require 5 to 25% of the energy compared with a standard hydrogen bond.[34] This is consistent with the Warburg effect which proposes that nonmalignant cells consume less energy than malignant cells.[35]

The other hypothesis that tumorous EVs are richer in β-sheets than EVs from nonmalignant origins, however, is not practical to prove by CD peaks because the spectra of predominant β-sheets have $\pi \rightarrow \pi^*$ transitions with magnitudes that are typically three to five times smaller than those generated by α-helix and thus are easily masked.[33] FT-IR spectroscopy measuring the wavelength and intensity of the absorption of IR radiation is another useful tool for determining the secondary structure of proteins.[36] The broad envelope of the amide I region (1700−1600 cm^{-1}) can be resolved to individual band components, which characterize the α-helical, β-sheet, and random content of the given proteins.[29,37] We thus investigated the protein secondary structure of the EVs through the second derivative IR spectra of the amide I band (Figure 1C left). EV changes in the protein secondary structure were witnessed by favoring α-helix (band component at 1653 cm^{-1}) or β-sheet conformations (1635 and 1644 cm^{-1}). The integrated intensity of the α-helix band with a peak at 1653 cm^{-1} as A_α and β-sheet with a peak at 1633 and 1644 as A_β were used to calculate the spectroscopic β-to-α ratio: A_α/A_β. Quantitative analysis by integrating each band elucidated that the β-sheet-to-α-helix ratio was significantly higher in tumorous EVs than normal ones (Figure 1C right). This is evidence to support the second hypothesis that the β-sheet is richer in the tumorous EV proteins.

To provide further evidence for the second hypothesis, we conducted thioflavin T (ThT) staining (Figure 1E). ThT is a proven tool to bind with β-sheets (Figure 1D), giving a strong fluorescence signal at approximately 482 nm when excited at 450 nm upon binding.[38−40] Fluorescence microscopy and flow cytometry results (Figure 1E,F left) confirmed the BR of the tumorous cells. EV level and cell lysate staining were detected under a fluorescence plate reader (Figure 1F), confirming the BR in tumorous EVs. These experimental observations (CD, FT-IR, and ThT staining), together, suggested that proteins in PDAC tumor cells and EVs are richer in β-sheets than their non-malignant counterparts.

β-Sheet Richness in Tumorous Cells and EVs by Counting Individual Proteins. CD, FT-IR spectrometry, and ThT staining assay reveal the aggregate attributes of protein in the EV and cell compartments without identifying individual proteins' contributions. We next investigated the secondary structure contribution of individual proteins. Modern mass spectrometry-based protein profiling introduces not only individual identification but also the quantitative information of individual protein contained in the sample, thus helping in comparative proteomics to enumerate the proteins in malignant and nonmalignant tissue at both cellular and EV levels. We designed a workflow to process proteomics result for the structural richness of the samples combining bioinformatics and simulation (Figure 2A). Briefly, each protein identified in the proteomics study was searched for in the protein databank (UniProt). The secondary structure information was used to calculate typical secondary structural configuration percentages for the protein. The primary sequence from the database was used in secondary structure prediction software to estimate the structural percentage. Since most of the proteins in the protein bank do not have completed secondary structure information, the final structural percentage of each protein was estimated using the following equation, $BP = pBP_{db} + (1 - p)BP_{sim}$, where p is the percentage of the sequence length with a known structure in the protein bank and BP_{db} and BP_{sim} are the β-sheet percentages (BPs) calculated from the protein database and simulation, respectively. The BR of a protein in the sample was defined as $BR = BP \cdot Q$, counting the relative quantity (Q) and BP of the protein. The BR of a sample was thus the sum of BR, denoted as $\sum BR$. Following the workflow, we reanalyzed our comparative proteomics result attained for one PDAC cell line [MIA PaCa-2 (M), malignant] and one immortalized normal human ductal epithelial cell line [HPNE (H), nonmalignant] at both EV and cellular levels.[41]

Pairing protein richness (defined as the percentage of individual proteins in the sample, Q) with the BP of the protein, the scatter plot (Figure 2B) demonstrates more β-sheet-rich proteins fell into the high richness quadrant (top-left) for malignant cells than nonmalignant counterparts. After removing all the overlapped proteins between nonmalignant and malignant cells, the same trend is observed. To obtain the collective structural richness counting individual protein's contribution, we investigated all secondary structures (α-helix, β-sheet, and random coil) at both cellular and EV levels following the workflow and similar calculation. Malignant cells and EVs contain higher BR ($\sum BR$) than nonmalignant counterparts (Figure 2C). This result confirms the higher BR of the malignant cells and EVs by investigating individual protein's structural contribution. Notably, both nonmalignant

https://doi.org/10.1021/acssensors.1c02022
ACS Sens. 2021, 6, 4489−4498

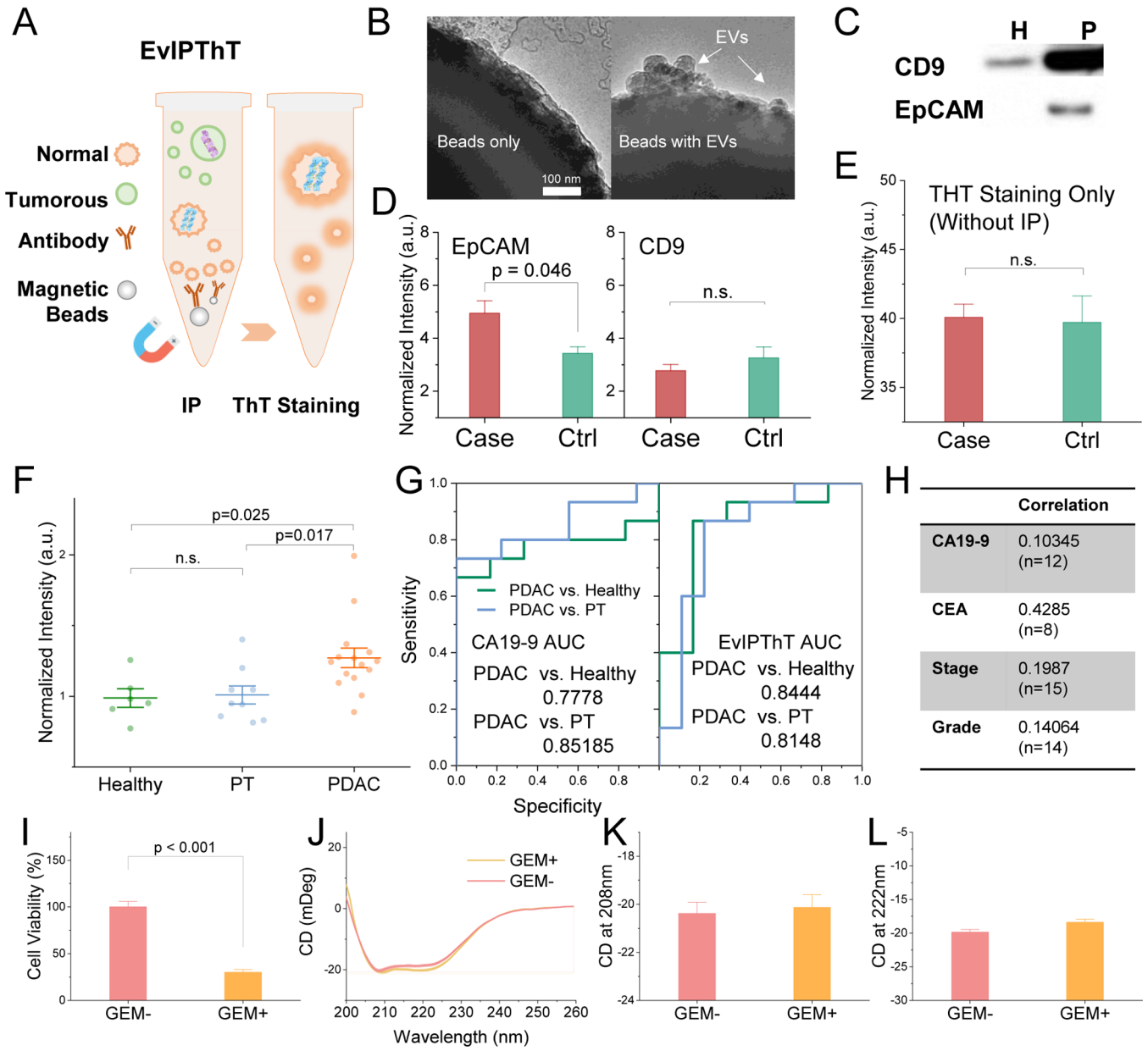

Figure 3. EvIPThT, a noninvasive screening option targeting tumorous EV BR. (A) Diagram of EvIPThT combining IP and ThT staining. (B) TEM images showing IP enrichment of EpCAM + EVs. (C) Western blotting analysis of EpCAM and CD9 in H and P cells. (D) Assay validation with anti-EpCAM and CD9 for IP. The case sample was constructed by spiking 5% EVs from PANC-1 cells into serum from a healthy donor. Control (ctrl): serum from the healthy donor ($n = 4$). (E) ThT staining only without IP for the case and ctrl sample ($n = 4$). (F) EvIPThT readout in healthy donors, PDAC, and pancreatitis (PT) patients (n = 6, 15, and 9, respectively). (G) ROC curve for EvIPThT from the pilot cohort. (H) Kendall correlation coefficients of EvIPThT to circulating CA19-9 and CEA, tumor stage and grade. (I) Viability of MIA PaCa-2 cells with and without gemcitabine (GEM) treatment (50 μM). (J–L) CD spectra, peak value at 222 and 208 nm (due to $\pi \rightarrow \pi^*$ and n $\rightarrow \pi^*$ transition, respectively), of the MIA PaCa-2 cellular proteins' CD spectra at a protein concentration of 0.5 mg/mL. H: HPNE; M: MIA PaCa-2; and P: PANC-1. Error bars, mean ± s.e.m; $n = 3$; n.s., not significant; and p values were determined by unpaired two-tailed t-tests.

and malignant cells exhibited higher BR at the cellular level than EVs, but the ratio differences between EV and cellular BR were similar (~82%). This observation suggests that passive exocytosis occurs from the cell into the EV with no sorting preference for β-sheet-rich proteins.

The abovementioned workflow potentiates a new analysis combining protein−protein interaction (PPI) information. We integrated the PPI result retrieved from the STRING[42] database to the proteomics result at the cellular level. It is noteworthy that the interactions are denser for proteins with high quantity within both nonmalignant and malignant cells (Figure 2D). The unbalanced interaction distribution of the malignant cells highlights the impact of the high abundance proteins to biological functions. We further combined PPI, BR, and relative quantity (Q) into circular network graphs (Figure 2E). Malignant cells presented a more complicated interaction network than nonmalignant. It advocates using collective attributes for cancer detection rather than a single protein hallmark, considering the complex protein−protein interaction context in tumor cells, making it difficult to attribute cancer development and progression to any one specific protein. This also explained why previous single markers have failed in various

https://doi.org/10.1021/acssensors.1c02022
ACS Sens. 2021, 6, 4489−4498

clinical situations to represent the complicated tumor cells, such as reporting false-positive.[43] Of note, the relative quantity (Q) of the protein dispersed over BP in nonmalignant cells but not in the malignant cells. Moreover, the denser interactions at a high BP (bottom-left corner) in malignant cells reveal the crucial effects of β-sheets on the biological functions of the tumor cell. These results suggest that β-sheet-rich proteins may play important roles in malignant cells, which endorse the secondary structure as a collective attribute to indicate the tumor cells' intricate homeostasis.

To gain functional insights into the β-sheet-rich proteins of tumor cells, gene ontology (GO) term enrichment analysis was conducted comparatively using the BRs of the proteome (Figure S1). With ΔE denoting the enrichment score difference between malignant and nonmalignant cells, GO enrichment analysis within local network cluster (LNC) (Figure 2F) showed the β-sheet preference in malignant cells. Specifically, proteins related to BCL2 associated agonist of cell death (BAD) activation anchored on the mitochondrion membrane[44] were β-sheet-enriched. Altered energy metabolism plays a central role in cancer development and progression, and increased mitochondrial abundance is a common characteristic of tumors that exhibit worse clinical outcomes.[45,46] Inspired by the enrichment analysis result, we next examined the BR over mitochondrial proteome (Figure 2G). Interestingly, both nonmalignant and malignant mitochondrial proteome showed higher BR than the cellular proteome (compared with Figure 2C). Since β-sheets consume more energy to fold, BR of the mitochondrion is consistent with its powerhouse organelle attribute. However, the richness difference between mitochondrial and cellular proteins (23.2 vs 20.2%) is higher in malignant cells. This result may explain the inefficiency of the aerobic glycolysis in tumor cells since more energy disperses in β-sheet-rich proteins of the mitochondrion.

Altogether, the workflow combining bioinformatics and simulation to analyze the proteomics result can serve as a de novo methodology. It validated the BR of the tumor cells at both cellular and EV levels by counting individual protein's contribution and enabled two further analyses PPI and enrichment analysis that links stereochemistry and biological function of the proteins, providing deeper insights into the tumor biology by means of energy distribution.

EvIPThT, Development of Clinical Method Using the Secondary Structure of Circulating EV Proteins. Although a significant secondary structure difference was observed between EV from nonmalignant and malignant origins, PDAC-derived EVs are expected to constitute a small fraction of the total serum EV population. Even for the malignant patients at the latest stage, tumorous EVs in the circulation system are comparatively minor. The signal from β-sheets contributed by these EVs could be masked by heterogeneous signals arising from the bulk of circulating EVs derived from nonmalignant cells.

To promote the secondary structure of the EV proteins for noninvasive clinical diagnostics and avoid the delicate instrumentation requirement for detection (e.g., CD or FITR), we developed a fluorescent assay with a combination of IP and ThT staining. In order to enrich tumor-derived EV for detection in serum samples, the IP method targeting tumor-derived EV's surface antigen was conducted before indicating BR of EV cargo proteins (including intravesicle and surface proteins) by ThT staining (schemed in Figure 3A), termed EvIPThT. IP is the canonical step that substantially saved time for EV isolation. Proven as a clinical method, the key factor of successful IP is the selection of membrane antigen. An epithelial cell adhesion molecule (EpCAM), an epithelial cell marker that is found overexpressed in PDAC tumors,[47−50] has been used to enrich tumor-derived EVs.[51,52] TEM images were used to validate the IP procedure for capturing tumorous EVs (Figure 3B). Western blotting (Figure 3C) was conducted to confirm the EpCAM expression on EVs from malignant cells (P), while common EV markers (CD9), a well-known pan EV surface marker used to isolate EVs,[53−55] expressed on EVs from both malignant and nonmalignant cells (H). To confirm the IP enrichment with anti-EpCAM in serum, case samples were constructed by spiking a trace amount (5%) of tumorous EVs into the healthy human serum, as cancer patient serum mimicry. Case samples showed significantly higher EvIPThT readout than control (healthy serum) with anti-EpCAM but not found with anti-CD9 (Figure 3D). Without IP enrichment, ThT staining alone could not discriminate case and control (Figure 3E), revealing the significant effect of IP enrichment in the assay. These data validate that tumorous EV with higher BR can be enriched by anti-EpCAM in serum and thus highlighted the clinical potency of using EvIPThT to differentiate cancer patients from healthy subjects.

We next conducted EvIPThT in a pilot cohort involving healthy control subjects, pancreatitis patients (PT), and pancreatic cancer (PDAC) patients with stage I−IV cancer. Analysis of the cohort revealed that the level of the EvIPThT readout distinguishes patients with histologically validated PDAC (n = 15) from healthy donors (n = 6) and patients with pancreatitis (PT; n = 9; Table S1). The receiver operating characteristic (ROC) curves in Figure 3G nominated EvIPThT readout as a potential classifier to distinguish PDAC cases from PT and healthy subjects (area under the curve, AUC, 0.84 vs 0.81). Compared with CA19-9, the clinical standard tumor prognosis marker for patients with PDAC,[56−58] EvIPThT assay was superior in distinguishing PDAC from healthy subjects (Table S2) but not PT. The EvIPThT level showed weak correlations to CA19-9 and CEA, suggesting a potential complementary method for diagnostics screening. CA19-9 and CEA are prevailing clinical prognosis markers, and their weak correlation to EvIPThT readout (Figure 3H) provides a hint that the secondary structure may not be affected by treatments. We, therefore, conducted in vitro treatment study. Malignant cells (MIA PaCa-2) treated with gemcitabine showed a dramatic decrease in viability (Figure 3I) but trivial CD spectrum change and thus the peak value at 222 and 208 nm (Figure 3J−L). These results confirmed the secondary structure might be irrelevant to treatment. High discriminatory power (PDAC vs healthy and PT), weak correlation to the pathological stage (AJCC), grade classifier, CA19-9 and CEA, and independence to treatment, together, suggested a potential clinical application of EvIPThT in PDAC screening. Further optimization to improve precision and repeatability, minimize time consumption, and achieve operational simplicity will be necessary for clinical translation.

DISCUSSION

Stereochemical properties play a prominent role in determining the function of the biomolecules and are widely used to evaluate the pharmacodynamic and pharmacokinetic properties of drugs, protein interactions, and the mechanisms of biorecognition.[59] With advanced X-ray diffraction and cryo-electron microscopy technology, the structures of numerous proteins have been determined at high resolution.[60] These structural explorations

https://doi.org/10.1021/acssensors.1c02022
ACS Sens. 2021, 6, 4489−4498

help in understanding the function of the proteins, however, presenting technical barriers for translational approaches. Intricate equipment, complex sample preparation process involving protein purification, and sophisticated operator necessity hindered the use of stereochemical information in clinical diagnosis and prognosis. Superior to the tertiary and quaternary structure of the proteins, which require elaborate measurement apparatus, the methods to evaluate the secondary structure are comparatively more accessible for clinical translation. Various direct and indirect approaches such as CD or nuclear magnetic resonance (NMR) are commonly used to explore the secondary structure.[61,62] However, the size, cost, and delicate nature of these systems limit their utility in field hospitals, clinical laboratories, and other settings where these factors become obstructive to translation. We studied the BR of EV proteins in relation to the malignancy because it can be captured noninvasively and quantified by fluorescence labeling, which is more feasible to be applied in clinical settings.

As shown in Figure 2E, a single protein marker is susceptible to other factors in the intricate protein−protein interactions, thus vulnerable to represent malignant cells' homeostasis with more complex interactions. This is the reason that we advocated collective attribute as a biomarker. Previously, we reported the nucleic acid-to-protein ratio of EV as a collective attribute for cancer detection.[41] In this study, we observed significant spectrometric differences (CD and FT-IR) between nonmalignant and malignant caused by β-sheets at both cellular and EV levels and further confirmed by fluorescence labeling. These experimental findings support the EV BR as a new noninvasive collective attribute marker.

Cancer cells exhibit an altered energy metabolism through aerobic glycolysis, even when provided with adequate oxygen. The alterations were considered to balance the need of the cell for energy with its equally important need for macromolecular building blocks and maintenance of redox balance.[63] Our observations provide a potential rationale for the superior energy demand of the cancer cells by protein folding. We found that malignant cells are richer in β-sheets and so is the exocytosis. Since β-sheets consume more energy to form the other secondary structures (α-helix and random coil), the biosynthesis of these β-sheet-rich proteins thus cost more energy in malignant cells. Although it cannot rule out the tertiary and quaternary structure's impact, our secondary structural findings highlighted a new analysis bridging the energy metabolism and stereochemical information.

Warburg theory advocated that mitochondrial abnormity plays a vital role in the development and progression of cancer. In PDAC cells, the abnormity exhibit enhanced mitochondria activity.[64] In our previous studies, we identified superior mitochondrial mass in PDAC cells (PANC-1, BxPC3, and MIA PaCa-2) than nonmalignant cells (HPNE).[41] Similarly, there are more mitochondrial DNA (mtDNA) in tumor cells at both the cellular and EV levels. Quantitatively elevated mitochondrial proteins from the proteomic study also featured the enhancement of mitochondrial activity in PDAC tumor cells. In this study, excessive β-sheet-rich mitochondrial proteins in malignant cells (Figure 2G) may serve as another manifestation of the Warburg effect.

In the functional enrichment analysis, we observed β-sheet enrichment in the activation of BAD, regulating protein insertion into the mitochondrial membrane of tumor cells (Figure 2F). Thus, these signals related to the apoptosis activation require more energy to function in tumor cells,[44] setting a higher energy barrier for activating programmed cell death to facilitate unrestricted growth. Tumor cells evolve these β-sheet-rich signals as defects in apoptosis, which might provide a survival advantage in the metabolic catastrophe that promotes tumorigenesis.[63]

PDAC has a 5-year survival rate of less than 5%, which has remained unchanged over the past 25 years.[65] Despite intensively studied, none of the available biomarkers possess a sufficiently high accuracy to be implemented for PDAC screening, even in high-risk patients. Serum CA19-9 as the most common clinical biomarker with a sensitivity of 70−80% but specificity less than 50% is currently employed as a treatment efficacy marker for PDAC rather than a diagnostic marker because of its correlation to tumor size and stage.[66,67] Recently, many biomarkers such as CEA, CA242, CA-125, MUC-1, CEACAM1, MIC-1, MMP-9, Lectins, REG4, osteopontin, k-ras mutation, and gene methylation were assessed for PDAC diagnosis.[67−69] However, considering both performance and implementation, serum CA19-9, although not satisfying, remains dominant in clinical practice. There is a need for the development of noninvasive but highly discriminatory methods for the detection of PDAC. We developed the clinically oriented assay, EvIPThT, to use the BR of circulating tumorous EV for screening. The assay consisted of IP and fluorescence detection, which are both well-accepted clinical methods, to solve the technical challenges for the new screening markers. High discrimination power and irrelevancy to the treatment featured the new assay as a candidate for PDAC screening complementary to the prevalent CA19-9. Further study is necessary to determine whether the EV BR is a specified marker for PDAC, adenocarcinoma, or a pan-cancer marker. However, the assay is flexible by switching the IP antibody to accommodate different types of cancer screening.

In summary, we confirmed the BR of the tumorous EV through CD measurement, FT-IR, and fluorescence labeling (ThT) and validated the experimental findings by combining quantitative proteomics result with secondary structure information from bioinformatics and simulation studies. Furthermore, we developed the finding into a PDAC screening assay, EvIPThT, integrated IP for tumorous EV enrichment in liquid biopsy, and ThT staining for labeling β-sheets. The combination featured with significant time saving (<0.75 h) compared with other EV detection involving EV isolation (e.g., ultracentrifugation > 3 h) and low sample consumption (100 μL serum). We found in our pilot study that EvIPThT readout presented high discriminatory power (PDAC vs healthy and PT) and weak correlations to the prognosis markers, suggesting cancer screening potential. Since both IP and fluorescence assays are automation-friendly and high-throughput, EvIPThT is seamlessly compatible with the current clinical laboratory setting, potentiating a feasible noninvasive cancer screening method.

METHODS

Detailed methods are provided in the Supporting Information.

ASSOCIATED CONTENT

Supporting Information

The Supporting Information is available free of charge at https://pubs.acs.org/doi/10.1021/acssensors.1c02022.

Materials and methods; functional enrichment analysis result; TEM images and unimodal size distributions of

https://doi.org/10.1021/acssensors.1c02022
ACS Sens. 2021, 6, 4489−4498

purified EVs from cell culture; dynamic range and linearity of ThT staining; impact of extravesicular protein contamination; linear response of EvIPThT; demographic information of the clinical cohort; accuracy of EvIPThT assay for screening PDAC from healthy; and characteristics of EvIPThT assay (PDF)

AUTHOR INFORMATION

Corresponding Author

Dali Sun − *Department of Electrical and Computer Engineering, North Dakota State University, Fargo, North Dakota 58102, United States; Biomedical Engineering Program, North Dakota State University, Fargo, North Dakota 58102, United States;* orcid.org/0000-0003-1691-2832; Email: dali.sun@ndsu.edu

Authors

Komila Rasuleva − *Department of Electrical and Computer Engineering, North Dakota State University, Fargo, North Dakota 58102, United States*

Santhalingam Elamurugan − *Biomedical Engineering Program, North Dakota State University, Fargo, North Dakota 58102, United States*

Aaron Bauer − *Biomedical Engineering Program, North Dakota State University, Fargo, North Dakota 58102, United States*

Mdrakibhasan Khan − *Department of Electrical and Computer Engineering, North Dakota State University, Fargo, North Dakota 58102, United States*

Qian Wen − *Department of Statistics, North Dakota State University, Fargo, North Dakota 58102, United States*

Zhaofan Li − *Department of Civil, Construction and Environmental Engineering, North Dakota State University, Fargo, North Dakota 58102, United States*

Preston Steen − *Sanford Roger Maris Cancer Center, Fargo, North Dakota 58122, United States*

Ang Guo − *Department of Pharmaceutical Sciences, North Dakota State University, Fargo, North Dakota 58102, United States*

Wenjie Xia − *Department of Civil, Construction and Environmental Engineering, North Dakota State University, Fargo, North Dakota 58102, United States;* orcid.org/0000-0001-7870-0128

Sijo Mathew − *Department of Pharmaceutical Sciences, North Dakota State University, Fargo, North Dakota 58102, United States*

Rick Jansen − *Department of Public Health, North Dakota State University, Fargo, North Dakota 58102, United States; Genomics and Bioinformatics Program, North Dakota State University, Fargo, North Dakota 58102, United States*

Complete contact information is available at: https://pubs.acs.org/10.1021/acssensors.1c02022

Author Contributions

D.S. conceived the idea, provided financial support, supervised the project, and conducted the experiments. K.R. and D.S. wrote the manuscript. K.R., S.E., A.B., and M.K. assisted with the experiments. D.S., A.G., P.S., W.X., R.J., and S.M. contributed to editing the manuscript. R.J. and Q.W. contributed to bioinformatics study. W.X. and Z.L. assisted in statistical analysis and graph. D.S. approved the final version of the manuscript.

Notes

The authors declare no competing financial interest.

Data and material availability: All data are available in the main text or the Supporting Information.

ACKNOWLEDGMENTS

The authors acknowledge North Dakota State University Center for Computationally Assisted Science and Technology (CCAST) for computing resources. This work was financially supported by grants from the National Cancer Institute (R03CA252783) and the National Institute of General Medical Sciences (U54GM128729) of National Institutes of Health to D.S., North Dakota State University (NDSU) COBRE Center for Diagnostic and Therapeutic Strategies in Pancreatic Cancer (1P20GM109024) to R.J., NDSU EPSCoR STEM Research and Education fund (FAR0032086) to D.S., ND EPSCoR: Advancing Science Excellence in ND (FAR0030554) to D.S., the National Science Foundation (NSF) under NSF EPSCoR Track-1 Cooperative Agreement (OIA #1355466) to D.S., the National Science Foundation (NSF) under NSF OIA ND-ACES (Award #1946202) to W.X., and NDSU Foundation and Alumni Association to D.S.

REFERENCES

(1) Camussi, G.; Deregibus, M. C.; Bruno, S.; Cantaluppi, V.; Biancone, L. Exosomes/Microvesicles as a Mechanism of Cell-to-Cell Communication. *Kidney Int.* **2010**, *78*, 838−848.

(2) Denzer, K.; Kleijmeer, M. J.; Heijnen, H. F.; Stoorvogel, W.; Geuze, H. J. Exosome: From Internal Vesicle of the Multivesicular Body to Intercellular Signaling Device. *J. Cell Sci.* **2000**, *113*, 3365−3374.

(3) Hannafon, B. N.; Ding, W.-Q. Cancer Stem Cells and Exosome Signaling. *Stem Cell Invest.* **2015**, *2*, 11.

(4) Valadi, H.; Ekström, K.; Bossios, A.; Sjöstrand, M.; Lee, J. J.; Lötvall, J. O. Exosome-Mediated Transfer of MRNAs and MicroRNAs Is a Novel Mechanism of Genetic Exchange between Cells. *Nat. Cell Biol.* **2007**, *9*, 654−659.

(5) Nazimek, K.; Ptak, W.; Nowak, B.; Ptak, M.; Askenase, P. W.; Bryniarski, K. Macrophages Play an Essential Role in Antigen-Specific Immune Suppression Mediated by t Cd8+ Cell-Derived Exosomes. *Immunology* **2015**, *146*, 23.

(6) Sung, B. H.; Ketova, T.; Hoshino, D.; Zijlstra, A.; Weaver, A. M. Directional Cell Movement through Tissues Is Controlled by Exosome Secretion. *Nat. Commun.* **2015**, *6*, 7164.

(7) Costa-Silva, B.; Aiello, N. M.; Ocean, A. J.; Singh, S.; Zhang, H.; Thakur, B. K.; Becker, A.; Hoshino, A.; Mark, M. T.; Molina, H.; Xiang, J.; Zhang, T.; Theilen, T.-M.; García-Santos, G.; Williams, C.; Ararso, Y.; Huang, Y.; Rodrigues, G.; Shen, T.-L.; Labori, K. J.; Lothe, I. M. B.; Kure, E. H.; Hernandez, J.; Doussot, A.; Ebbesen, S. H.; Grandgenett, P. M.; Hollingsworth, M. A.; Jain, M.; Mallya, K.; Batra, S. K.; Jarnagin, W. R.; Schwartz, R. E.; Matei, I.; Peinado, H.; Stanger, B. Z.; Bromberg, J.; Lyden, D. Pancreatic Cancer Exosomes Initiate Pre-Metastatic Niche Formation in the Liver. *Nat. Cell Biol.* **2015**, *17*, 816−826.

(8) Yoshioka, Y.; Kosaka, N.; Konishi, Y.; Ohta, H.; Okamoto, H.; Sonoda, H.; Nonaka, R.; Yamamoto, H.; Ishii, H.; Mori, M.; Furuta, K.; Nakajima, T.; Hayashi, H.; Sugisaki, H.; Higashimoto, H.; Kato, T.; Takeshita, F.; Ochiya, T. Ultra-Sensitive Liquid Biopsy of Circulating Extracellular Vesicles Using ExoScreen. *Nat. Commun.* **2014**, *5*, 3591.

(9) McGuire, A.; Brown, J. A. L.; Kerin, M. J. Metastatic Breast Cancer: The Potential of MiRNA for Diagnosis and Treatment Monitoring. *Cancer Metastasis Rev.* **2015**, *34*, 145−155.

(10) Wang, X.; Zhong, W.; Bu, J.; Li, Y.; Li, R.; Nie, R.; Xiao, C.; Ma, K.; Huang, X.; Li, Y. Exosomal Protein CD82 as a Diagnostic Biomarker for Precision Medicine for Breast Cancer. *Mol. Carcinog.* **2019**, *58*, 674−685.

(11) Sheridan, C. Exosome Cancer Diagnostic Reaches Market. *Nat. Biotechnol.* **2016**, *34*, 359−360.

(12) Sun, D.; Yang, L.; Lyon, C. J.; Hu, T. Simulation-Directed Amplifiable Nanoparticle Enhanced Quantitative Scattering Assay under Low Magnification Dark Field Microscopy. *J. Mater. Chem. B* **2020**, *8*, 5416.
(13) Sun, D.; Fan, J.; Liu, C.; Liu, Y.; Bu, Y.; Lyon, C. J.; Hu, Y. Noise Reduction Method for Quantifying Nanoparticle Light Scattering in Low Magnification Dark-Field Microscope Far-Field Images. *Anal. Chem.* **2016**, *88*, 12001−12005.
(14) Sun, D.; Hu, T. Y. A Low Cost Mobile Phone Dark-Field Microscope for Nanoparticle-Based Quantitative Studies. *Biosens. Bioelectron.* **2018**, *99*, 513−518.
(15) Masyuk, A. I.; Masyuk, T. V.; Larusso, N. F. Exosomes in the Pathogenesis, Diagnostics and Therapeutics of Liver Diseases. *J. Hepatol.* **2013**, *59*, 621−625.
(16) He, W.; Kularatne, S. A.; Kalli, K. R.; Prendergast, F. G.; Amato, R. J.; Klee, G. G.; Hartmann, L. C.; Low, P. S. Quantitation of Circulating Tumor Cells in Blood Samples from Ovarian and Prostate Cancer Patients Using Tumor-Specific Fluorescent Ligands. *Int. J. Cancer* **2008**, *123*, 1968.
(17) Yang, K. S.; Im, H.; Hong, S.; Pergolini, I.; del Castillo, A. F.; Wang, R.; Clardy, S.; Huang, C.-H.; Pille, C.; Ferrone, S.; Yang, R.; Castro, C. M.; Lee, H.; del Castillo, C. F.; Weissleder, R. Multiparametric Plasma EV Profiling Facilitates Diagnosis of Pancreatic Malignancy. *Sci. Transl. Med.* **2017**, *9*, No. eaal3226.
(18) Qin, X.-L.; Wang, Z.-R.; Shi, J.-S.; Lu, M.; Wang, L.; He, Q.-R. Utility of Serum CA19-9 in Diagnosis of Cholangiocarcinoma: In Comparison with CEA. *World J. Gastroenterol.* **2004**, *10*, 427−432.
(19) Marrelli, D.; Caruso, S.; Pedrazzani, C.; Neri, A.; Fernandes, E.; Marini, M.; Pinto, E.; Roviello, F. CA19-9 Serum Levels in Obstructive Jaundice: Clinical Value in Benign and Malignant Conditions. *Am. J. Surg.* **2009**, *198*, 333−339.
(20) Lange, H.; Zuber, H.; Sement, F. M.; Chicher, J.; Kuhn, L.; Hammann, P.; Brunaud, V.; Bérard, C.; Bouteiller, N.; Balzergue, S.; Aubourg, S.; Martin-Magniette, M.-L.; Vaucheret, H.; Gagliardi, D. The RNA Helicases AtMTR4 and HEN2 Target Specific Subsets of Nuclear Transcripts for Degradation by the Nuclear Exosome in Arabidopsis Thaliana. *PLoS Genet.* **2014**, *10*, No. e1004564.
(21) Lubas, M.; Andersen, P. R.; Schein, A.; Dziembowski, A.; Kudla, G.; Jensen, T. H. The Human Nuclear Exosome Targeting Complex Is Loaded onto Newly Synthesized RNA to Direct Early Ribonucleolysis. *Cell Rep.* **2015**, *10*, 178−192.
(22) Im, H.; Shao, H.; Park, Y. I.; Peterson, V. M.; Castro, C. M.; Weissleder, R.; Lee, H. Label-Free Detection and Molecular Profiling of Exosomes with a Nano-Plasmonic Sensor. *Nat. Biotechnol.* **2014**, *32*, 490−495.
(23) Maas, S. L. N.; Broekman, M. L. D.; de Vrij, J. Tunable Resistive Pulse Sensing for the Characterization of Extracellular Vesicles. *Methods Mol. Biol.* **2017**, *1545*, 21−33.
(24) Coumans, F. A. W.; van der Pol, E.; Böing, A. N.; Hajji, N.; Sturk, G.; van Leeuwen, T. G.; Nieuwland, R. Reproducible Extracellular Vesicle Size and Concentration Determination with Tunable Resistive Pulse Sensing. *J. Extracell. Vesicles* **2014**, *3*, 25922.
(25) Momen-Heravi, F.; Balaj, L.; Alian, S.; Tigges, J.; Toxavidis, V.; Ericsson, M.; Distel, R. J.; Ivanov, A. R.; Skog, J.; Kuo, W. P. Alternative Methods for Characterization of Extracellular Vesicles. *Front. Physiol.* **2012**, *3*, 354.
(26) Gardiner, C.; Ferreira, Y. J.; Dragovic, R. A.; Redman, C. W. G.; Sargent, I. L. Extracellular vesicle sizing and enumeration by nanoparticle tracking analysis. *J. Extracell. Vesicles* **2013**, *2*, 19671.
(27) Bachurski, D.; Schuldner, M.; Nguyen, P.-H.; Malz, A.; Reiners, K. S.; Grenzi, P. C.; Babatz, F.; Schauss, A. C.; Hansen, H. P.; Hallek, M.; Pogge von Strandmann, E. Extracellular Vesicle Measurements with Nanoparticle Tracking Analysis−An Accuracy and Repeatability Comparison between NanoSight NS300 and ZetaView. *J. Extracell. Vesicles* **2019**, *8*, 1596016.
(28) Vestad, B.; Llorente, A.; Neurauter, A.; Phuyal, S.; Kierulf, B.; Kierulf, P.; Skotland, T.; Sandvig, K.; Haug, K. B. F.; Øvstebø, R. Size and concentration analyses of extracellular vesicles by nanoparticle tracking analysis: a variation study. *J. Extracell. Vesicles* **2017**, *6*, 1344087.
(29) Krafft, C.; Wilhelm, K.; Eremin, A.; Nestel, S.; von Bubnoff, N.; Schultze-Seemann, W.; Popp, J.; Nazarenko, I. A Specific Spectral Signature of Serum and Plasma-Derived Extracellular Vesicles for Cancer Screening. *Nanomedicine* **2017**, *13*, 835−841.
(30) Miles, A. J.; Wallace, B. A. Circular dichroism spectroscopy of membrane proteins. *Chem. Soc. Rev.* **2016**, *45*, 4859−4872.
(31) Greenfield, N. J. Using Circular Dichroism Spectra to Estimate Protein Secondary Structure. *Nat. Protoc.* **2007**, *1*, 2876−2890.
(32) Nagy, G.; Igaev, M.; Hoffmann, S. V.; Jones, N. C.; Grubmüller, H. SESCA: Predicting the Circular Dichroism Spectra of Proteins from Molecular Structure. *J. Chem. Theory Comput.* **2019**, *15* (9), 5087−5102.
(33) Miles, A. J.; Wallace, B. A. Circular Dichroism Spectroscopy of Membrane Proteins. *Chem. Soc. Rev.* **2016**, *45* (18), 4859−4872.
(34) Martz, E. Introduction to Proteins-Structure, Function, and Motion. *Biochem. Mol. Biol. Educ.* **2012**, *40*, 218.
(35) Fadaka, A.; Ajiboye, B.; Ojo, O.; Adewale, O.; Olayide, I.; Emuowhochere, R. Biology of Glucose Metabolization in Cancer Cells. *J. Oncol. Sci.* **2017**, *3*, 45−51.
(36) Yang, H.; Yang, S.; Kong, J.; Dong, A.; Yu, S. Obtaining Information about Protein Secondary Structures in Aqueous Solution Using Fourier Transform IR Spectroscopy. *Nat. Protoc.* **2015**, *10*, 382−396.
(37) Mihály, J.; Deák, R.; Szigyártó, I. C.; Bóta, A.; Beke-Somfai, T.; Varga, Z. Characterization of Extracellular Vesicles by IR Spectroscopy: Fast and Simple Classification Based on Amide and C[Sbnd]H Stretching Vibrations. *Biochim. Biophys. Acta, Biomembr.* **2017**, *1859*, 459−466.
(38) Xue, C.; Lin, T. Y.; Chang, D.; Guo, Z. Thioflavin T as an amyloid dye: fibril quantification, optimal concentration and effect on aggregation. *R. Soc. Open Sci.* **2017**, *4*, 160696.
(39) Sulatskaya, A. I.; Lavysh, A. V.; Maskevich, A. A.; Kuznetsova, I. M.; Turoverov, K. K. Thioflavin T Fluoresces as Excimer in Highly Concentrated Aqueous Solutions and as Monomer Being Incorporated in Amyloid Fibrils. *Sci. Rep.* **2017**, *7*, 1−11.
(40) Passarella, D.; Goedert, M. Beta-Sheet Assembly of Tau and Neurodegeneration in Drosophila Melanogaster. *Neurobiol. Aging* **2018**, *72*, 98−105.
(41) Sun, D.; Zhao, Z.; Spiegel, S.; Liu, Y.; Fan, J.; Amrollahi, P.; Hu, J.; Lyon, C. J.; Wan, M.; Hu, T. Y. Dye-Free Spectrophotometric Measurement of Nucleic Acid-to-Protein Ratio for Cell-Selective Extracellular Vesicle Discrimination. *Biosens. Bioelectron.* **2021**, *179*, 113058.
(42) Szklarczyk, D.; Morris, J. H.; Cook, H.; Kuhn, M.; Wyder, S.; Simonovic, M.; Santos, A.; Doncheva, N. T.; Roth, A.; Bork, P.; Jensen, L. J.; von Mering, C. The STRING Database in 2017: Quality-Controlled Protein-Protein Association Networks, Made Broadly Accessible. *Nucleic Acids Res.* **2017**, *45*, D362−D368.
(43) Xu, H.-X.; Liu, L.; Xiang, J.-F.; Wang, W.-Q.; Qi, Z.-H.; Wu, C.-T.; Liu, C.; Long, J.; Xu, J.; Ni, Q.-X.; Yu, X.-J. Postoperative Serum CEA and CA125 Levels Are Supplementary to Perioperative CA19-9 Levels in Predicting Operative Outcomes of Pancreatic Ductal Adenocarcinoma. *Surg* **2017**, *161*, 373−384.
(44) Basu Mallik, S.; Jayashree, B. S.; Shenoy, R. R. Epigenetic Modulation of Macrophage Polarization- Perspectives in Diabetic Wounds. *J. Diabetes Complicat.* **2018**, *32*, 524−530.
(45) Carew, J. S.; Huang, P. Mitochondrial Defects in Cancer. *Mol. Cancer* **2002**, *1*, 9−12.
(46) Vyas, S.; Zaganjor, E.; Haigis, M. C. Mitochondria and Cancer. *Cell* **2016**, *166*, 555−566.
(47) Andre, F.; Schartz, N. E.; Movassagh, M.; Flament, C.; Pautier, P.; Morice, P.; Pomel, C.; Lhomme, C.; Escudier, B.; Le Chevalier, T.; Tursz, T.; Amigorena, S.; Raposo, G.; Angevin, E.; Zitvogel, L. Malignant Effusions and Immunogenic Tumour-Derived Exosomes. *Lancet* **2002**, *360*, 295−305.
(48) Maetzel, D.; Denzel, S.; Mack, B.; Canis, M.; Went, P.; Benk, M.; Kieu, C.; Papior, P.; Baeuerle, P. A.; Munz, M.; Gires, O. Nuclear

Signalling by Tumour-Associated Antigen EpCAM. *Nat. Cell Biol.* **2009**, *11*, 162.
(49) Went, P. T. H.; Lugli, A.; Meier, S.; Bundi, M.; Mirlacher, M.; Sauter, G.; Dirnhofer, S. Frequent EpCam Protein Expression in Human Carcinomas. *Hum. Pathol.* **2004**, *35*, 122.
(50) Kosti, I.; Jain, N.; Aran, D.; Butte, A. J.; Sirota, M. Cross-Tissue Analysis of Gene and Protein Expression in Normal and Cancer Tissues. *Sci. Rep.* **2016**, *6*, 1−16.
(51) Zhang, J.; Li, S.; Li, L.; Li, M.; Guo, C.; Yao, J.; Mi, S. Exosome and Exosomal MicroRNA: Trafficking, Sorting, and Function. *Genomics, Proteomics Bioinf.* **2015**, *13*, 17−24.
(52) Li, A.; Zhang, T.; Zheng, M.; Liu, Y.; Chen, Z. Exosomal Proteins as Potential Markers of Tumor Diagnosis. *J. Hematol. Oncol.* **2017**, *10*, 1−9.
(53) Li, P.; Kaslan, M.; Lee, S. H.; Yao, J.; Gao, Z. Progress in Exosome Isolation Techniques. *Theranostics* **2017**, *7*, 789.
(54) Hurwitz, S. N.; Rider, M. A.; Bundy, J. L.; Liu, X.; Singh, R. K.; Meckes, D. G. Proteomic Profiling of NCI-60 Extracellular Vesicles Uncovers Common Protein Cargo and Cancer Type-Specific Biomarkers. *Oncotarget* **2016**, *7*, 86999−87015.
(55) Azmi, A. S.; Bao, B.; Sarkar, F. H. Exosomes in Cancer Development, Metastasis, and Drug Resistance: A Comprehensive Review. *Cancer Metastasis Rev.* **2013**, *32*, 623−642.
(56) Hess, V.; Glimelius, B.; Grawe, P.; Dietrich, D.; Bodoky, G.; Ruhstaller, T.; Bajetta, E.; Saletti, P.; Figer, A.; Scheithauer, W.; Herrmann, R. CA 19-9 Tumour-Marker Response to Chemotherapy in Patients with Advanced Pancreatic Cancer Enrolled in a Randomised Controlled Trial. *Lancet Oncol.* **2008**, *9*, 132.
(57) E. Poruk, K.; Brown, K.; M. Boucher, K.; L. Scaife, C.; J. Mulvihill, S. The Clinical Utility of CA 19-9 in Pancreatic Adenocarcinoma: Diagnostic and Prognostic Updates. *Curr. Mol. Med.* **2013**, *13*, 340−351.
(58) Distler, M.; Pilarsky, E.; Kersting, S.; Grützmann, R. Preoperative CEA and CA 19-9 Are Prognostic Markers for Survival after Curative Resection for Ductal Adenocarcinoma of the Pancreas - A Retrospective Tumor Marker Prognostic Study. *Int. J. Surg.* **2013**, *11*, 1067−1072.
(59) Bertucci, C.; Pistolozzi, M.; De Simone, A. Circular Dichroism in Drug Discovery and Development: An Abridged Review. *Anal. Bioanal. Chem.* **2010**, *398*, 155−166.
(60) Shoemaker, S. C.; Ando, N. X-rays in the Cryo-Electron Microscopy Era: Structural Biology's Dynamic Future. *Biochemistry* **2018**, *57*, 277−285.
(61) Böselt, L.; Sidler, D.; Kittelmann, T.; Stohner, J.; Zindel, D.; Wagner, T.; Riniker, S. Determination of Absolute Stereochemistry of Flexible Molecules Using a Vibrational Circular Dichroism Spectra Alignment Algorithm. *J. Chem. Inf. Model.* **2019**, *59*, 1826.
(62) Pelton, J. T.; McLean, L. R. Spectroscopic Methods for Analysis of Protein Secondary Structure. *Anal. Biochem.* **2000**, *277*, 167−176.
(63) Cairns, R. A.; Harris, I. S.; Mak, T. W. Regulation of Cancer Cell Metabolism. *Nat. Rev. Cancer* **2011**, *11*, 85−95.
(64) Bryant, K. L.; Mancias, J. D.; Kimmelman, A. C.; Der, C. J. KRAS: Feeding Pancreatic Cancer Proliferation. *Trends Biochem. Sci.* **2014**, *39*, 91−100.
(65) Lockhart, A. C.; Rothenberg, M. L.; Berlin, J. D. Treatment for Pancreatic Cancer: Current Therapy and Continued Progress. *Gastroenterology* **2005**, *128*, 1642−1654.
(66) Pfister, M.; Gottstein, B.; Kretschmer, R.; Cerny, T.; Cerny, A. Elevated Carbohydrate Antigen 19-9 (CA 19-9) in Patients with Echinococcus Infection. *Clin. Chem. Lab. Med.* **2001**, *39*, 527−530.
(67) Liu, J.; Gao, J.; Du, Y.; Li, Z.; Ren, Y.; Gu, J.; Wang, X.; Gong, Y.; Wang, W.; Kong, X. Combination of Plasma MicroRNAs with Serum CA19-9 for Early Detection of Pancreatic Cancer. *Int. J. Cancer* **2012**, *131*, 683−691.
(68) Chari, S. T.; Kelly, K.; Hollingsworth, M. A.; Thayer, S. P.; Ahlquist, D. A.; Andersen, D. K.; Batra, S. K.; Brentnall, T. A.; Canto, M.; Cleeter, D. F.; Firpo, M. A.; Gambhir, S. S.; Go, V. L. W.; Hines, O. J.; Kenner, B. J.; Klimstra, D. S.; Lerch, M. M.; Levy, M. J.; Maitra, A.; Mulvihill, S. J.; Petersen, G. M.; Rhim, A. D.; Simeone, D. M.; Srivastava, S.; Tanaka, M.; Vinik, A. I.; Wong, D. Early Detection of Sporadic Pancreatic Cancer. *Pancreas* **2015**, *44*, 693−712.
(69) Warton, K.; Samimi, G. Methylation of Cell-Free Circulating DNA in the Diagnosis of Cancer. *Front. Mol. Biosci.* **2015**, *2*, 1−10.

https://doi.org/10.1021/acssensors.1c02022
ACS Sens. 2021, 6, 4489−4498